Shape-CD: Change-Point Detection in Time-Series Data with Shapes and Neurons

Varsha Suresh
School of Computing
National University of Singapore
Singapore
varshasuresh@u.nus.edu

Wei Tsang Ooi
School of Computing
National University of Singapore
Singapore
ooiwt@comp.nus.edu.sg

***Abstract*—Change-point detection in a time series aims to discover the time points at which some unknown underlying physical process that generates the time-series data has changed. We found that existing approaches become less accurate when the underlying process is complex and generates large varieties of patterns in the time series. To address this shortcoming, we propose Shape-CD, a simple, fast, and accurate change point detection method. Shape-CD uses shape-based features to model the patterns and a conditional neural field to model the temporal correlations among the time regions. We evaluated the performance of Shape-CD using four highly dynamic time-series datasets, including the ExtraSensory dataset with up to 2000 classes. Shape-CD demonstrated improved accuracy (7-60% higher in AUC) and faster computational speed compared to existing approaches. Furthermore, the Shape-CD model consists of only hundreds of parameters and require less data to train than other deep supervised learning models.**

***Index Terms*—Change-point detection, Time-series, Shape, Conditional Neural Field.**

I. Introduction

Change-point detection is one of the fundamental problems in time series analysis and has many applications including in environmental science [1], healthcare [2], financial analysis [3] and human activity analysis [4]. The goal of change-point detection is to identify the time points at which the underlying physical process that generates the time series data has changed, by analyzing only the observed time series data, without knowing the underlying process. Given its importance, there has been a plethora of work on change-point detection in time-series data (see Aminikhanghahi and Cook [5] for a recent survey).

We found, however, that the existing approaches failed to perform adequately when the underlying process is complex and generates a large variety of different patterns in the observed time series data. A case in point, which motivates our work in this paper, is the tri-axial accelerometer data collected in-the-wild for daily human activity detection. The ExtraSensory dataset [6] that captures such data, for instance, has up to 2,000 classes of human activities. Each activity can further generate multiple patterns of movement, leading to different patterns in the time-series data.

Existing approaches for change point detection can fail to perform in such highly complex time series. Approaches that rely on statistical features such as mean and variance [7], [8] do not perform well since data generated by physical process can be non-stationary in nature, that is, the statistical properties of the data might evolve over time [9], [10]. Approaches that model the data generation process, using either reference probability distributions [11], [12], state-space models [7], [13], or auto-regressive models [14], track changes in the parameters of the model to compute the change score. When the underlying data generation process is complex, however, identifying the underlying model becomes challenging. Density ratio estimation methods [15], [16], [17], on the other hand, directly estimate the probability density ratios between the adjacent time intervals and compare them with a divergence metric to obtain change scores. These methods need to compare the change scores against a preset threshold in order to detect a change. When the underlying data generation process is as complex as human activities, we found that using a single threshold does not work well. Finally, supervised learning-based approaches learn to map a time series to two or more classes. In the case of multi-class classification, transitions are considered as either a change in the predicted output class or one of the output classes [18], [19], [20]. Multi-class classification does not scale well as the number of classes increases, as the learning model needs to be more complex and needs more training data to learn well. Alternatively, binary classification methods simply learn to predict whether or not a change occurred [21], [22]. While these methods no longer suffer due to the number of classes, learning a suitable model can still be difficult since a change can be caused by many possible underlying events, and two time regions that belongs to the same class which should be classified as "no change" may also exhibit significant differences in the time-series data, complicating the distinction between the two classes. Despite the shortcomings of existing binary classification-based methods, we find that this is the most promising approach, and our method presented here falls under this category.

Our method, called *Shape-CD*, is a supervised binary classification-based method that combines two well-known techniques: shape-based features (using dynamic time warping [23]) and conditional neural field [24]. Previous works have identified interval-specific temporal properties such as the shape of a sub-sequence to be a more meaningful rep-

resentation of the time series than statistical features for classification and clustering [25]. Drawing inspiration, Shape-CD uses dissimilarity in shape between adjacent time intervals as a feature for detecting change points. Pairing this dissimilarity score with a threshold to determine a change, however, would not work, due to the dynamics and complexity of the data generation process. In the context of human activities, for instance, a single threshold would not work for changes between any two activities. Furthermore, activities, such as eating, that generates multiple dissimilar patterns would lead to false positives. Instead of looking at two adjacent time regions, Shape-CD learns about temporal correlations of dissimilarities of past region to classify a region as a change point or not. Furthermore, due to the complexity of the data generation process, the dissimilarity between the different variables/dimensions of the time series are likely not linearly correlated. To this end, Shape-CD uses conditional neural field, a conditional probabilistic graphical model for sequence labeling, to learn about the non-linear relationship between the dissimilarities of different time-series dimensions and the temporal correlations between past time regions.

Despite the rather straightforward combinations of the two known methods, we are surprised that (i) no one in the literature has reported this before, and (ii) it works incredibly well, both in terms of speed and accuracy, on the complex ExtraSensory dataset and three other datasets we tried. In particular, Shape-CD exhibits up to 21% higher area-under-the-curve (AUC) on the ExtraSensory dataset and 38% higher AUC on the DCASE dataset compared to the state-of-the-art method KL-CPD [26]; It is also 42% higher AUC on the Bee Dance dataset compared to RuLSIF. Shape-CD also has a relatively simpler model, with only a few hundreds parameters, which is order of magnitudes smaller than LSTM, while achiving up 25% - 61% higher AUC.

The rest of the paper is organized as follows. Section II discusses the existing works related to change point detection in time series. Section III formally defines the problem of change point detection. Section IV describes Shape-CD and the conditional neural field model that it uses. This section is followed by the detailed evaluation of our approach in Section V on four real-world datasets to illustrate its performance in terms of both accuracy and speed. We also perform a parameter sensitivity analysis to understand the effect of different parameter setting on our model's performance. We conclude the paper in Section VI.

II. Related Work

We now present the existing approaches to change point detection in time series data in more details. We broadly group the existing approaches into two categories: unsupervised and supervised approaches.

A. Unsupervised Approaches

Unsupervised approaches for change point detection such as CUSUM [11] and Generalised Likelihood Ratio (GLR) [12] define the generation of data using known distributions where the parameters before a change occurs are usually assumed to be known. In these methods, the log-likelihood ratio between adjacent time segments serve as the measure for change point detection. The main challenge posed by the above approaches, however, was accurate estimation of these probability densities. To circumvent this, methods such as Kullback-Leibler Importance Estimation Procedure (KLIEP) [15], Unconstrained Least Square Importance Fitting (uLSIF) [16] and Relative Unconstrained Least Square Importance Fitting (RuLSIF) [17] estimate the density ratio directly instead of determining the densities separately. The main advantage of these approaches is their data independence. Nonetheless, they require a preset threshold to detect the change. Some approaches have tried to model the data generation using state-space models [7], [13] or auto regressive models [14]. In the former, a change is determined by comparing the sub-spaces obtained using Principal Component Analysis (PCA) from the past and present time intervals to a pre-defined threshold. Auto Regression (AR) methods model the data as an AR model, which represents the statistical behavior of the time series. Change is detected by tracking the statistical behaviour of the time series.

A closely related line of work are the kernel-based techniques for change detection. The detection rule in these set of approaches is done by comparing the homogeneity before and after a change using a distance metric such as KFDR (Kernel Fisher Discriminant Ratio) [8]. However, they are sensitive to the choice of kernel and also suffer from the curse of dimensionality [27]. A recent work KL-CPD (Kernel Learning Change Point Detection) [26] overcame this by learning the kernels directly from the data using a combination of RNN (Recurrent Neural Networks) and RBF (Radial Basis Function) kernels. The authors have shown that KL-CPD achieves state-of-the-art performance making it the main baseline for comparison against our method.

All the above unsupervised approaches work well when either adequate pre-determined models such as underlying probability distributions, state space models, and AR models can be defined, or when apt thresholds to determine change are available. In realistic scenarios, however, it is not straightforward to determine such a static threshold or a model that works for all changes even within a specific application.

B. Supervised Approaches

Supervised methods, on the other hand, learn a direct mapping from input to output class. One set of supervised approaches learn a model that can classify all the possible states of the time series and when the classification output changes between time intervals, it is identified as a change. Various models such as Support Vector Machines (SVM) [4], Relational Markov Networks (RMN) [19] and Long Short Term Memory (LSTM) [22], [20] have been used as multi-class change detectors. They have been shown to perform robustly in application-centric situations with fewer class labels. As the number of output classes increases, the amount of variations present in the data increases. This issue can make the models become increasingly complex.

The second set of approaches [21], [22] learn to predict between two classes; change and no change. Change detection in this manner, however, can become cumbersome as all the varied changes occurring within the data are attributed to one class, i.e., "change" [5]. Using representative features help in this regard to guide the model better to improve its performance.

In summary, change is relative, i.e., it is said to have occurred only when the current interval properties of a time series appear different from those from the previous intervals. Unsupervised methods naturally capture this relative difference using the change scores between adjacent time intervals. The necessity of a pre-determined threshold, however, makes them less flexible in practice. Orthogonally, supervised approaches have been successful in detecting domain specific changes. For this, however, increasingly complex models are required to learn the multitude of variations present in the data and this in turn requires large amounts data to train.

III. Change Point Detection

We start by defining the problem of change point detection. Let $x_i \in \mathbb{R}^d$ be a d-dimensional time series sample at time instant i. Then, the t^{th} time-series region of length k is given by $\vec{x}_t = \langle x_j \rangle_{j=(t-1)k}^{tk-1}$. A time series that is segmented into non-overlapping time regions, each of size k, can be written as $\langle \vec{x}_t \rangle_{t=1}^{T}$, where the total length of the time series is Tk. Note that, we use the terms regions and segments interchangeably. We refer to $\vec{x}_t$ as the observation at time instant t.

We assume the underlying process that generates the data as being in some discrete state at any time instance. Without loss of generality, we assume that the process is in the same state throughout a time region (we can pick the most common state the process is in otherwise, breaking ties arbitrarily). Denoting s_t as the state of the process in the t^{th} time region. The t^{th} time region is a change point if $s_t \neq s_{t-1}$. We define

$$y_t = \begin{cases} 1 & \text{if } s_{t-1} \neq s_t \\ 0 & \text{otherwise.} \end{cases} \tag{1}$$

We refer to y_t as the (true) output/hidden state.

The state s_t of the underlying process determines the observations $\vec{x}_t$. The challenge of change point detection is to determine y_t only via $\vec{x}_t$ without knowing the state s_t or the relationship between s_t and $\vec{x}_t$ a priori. Denote $\hat{y}_t$ as the inferred output state. Our goal is thus to compute $\hat{y}_t$ for each t to minimize the errors, through the objective function given by:

$$\min_{\hat{y}} \mathbb{E}\left[\sum_{t=1}^{T} \mathbb{1}_{\hat{y}_t \neq y_t}\right]$$

where $\mathbb{1}_{\hat{y}_t \neq y_t}$ is an indicator function which outputs 1 if $\hat{y}_t \neq y_t$ and 0 otherwise.

IV. Shape-CD

In this section, we will first present how we extract shape-based features, followed by a preliminary of computational neural field. We end the section by describing how Shape-CD combines both to yield a robust method for change point detection.

A. Shape-dissimilarity based feature

The shape of a signal has been widely used for clustering and classification [28], [29], [30], [31], [32]. The definition of *shape* is dependent on the distance metric used. In many applications, metrics that can handle multiple inherent distortions in the data is preferred. Dynamic time warping, or DTW, is widely used as a shape-based distance measure. When combined with 1-NN (Nearest Neighbour), DTW gives the state-of-the-art performance in time-series classification [33]. Given its strength in capturing the properties of time series, we choose shape-based features to measure dissimilarity between adjacent time regions and capture changes in the time-series patterns.

Shape-CD uses FastDTW [34], which is an approximate version of DTW for faster computation. FastDTW introduces a multilevel approach that repeatedly projects the DTW path to finer resolutions and then refines this solution. As the time series unfolds, the length of path increases linearly with the length of the time series, enabling it to have linear time and space complexity. Despite what is reported in the literature [35], we found that FastDTW is much faster than classic DTW[1].

In addition to that, we modified FastDTW to relax the end-point constraints [36], [37], which in turn allows some misalignment in the end points of the time regions when matching the sub-sequences. The relaxation is parameterized by a factor r, which represents the allowance of offset in the start and end points.

In reference to our problem, let's represent the relaxed FastDTW distance function as $\mathcal{F}_k(\vec{x}_{t-1}, \vec{x}_t, r)$, which finds similarity between time regions at t and $t-1$ along dimension k. The feature function $D_k(\vec{x}_{t-1}, \vec{x}_t)$ computes the distance score by using the difference between the relaxed FastDTW scores at time instants $t-1$ and t, which the distance is measured. This can be written as,

$$D_{k,t} = D_k(\vec{x}_{t-1}, \vec{x}_t) = \mathcal{F}_k(\vec{x}_{t-2}, \vec{x}_{t-1}, r) - \mathcal{F}_k(\vec{x}_{t-1}, \vec{x}_t, r) \tag{2}$$

Therefore, in the case of a d-dimensional time-series data, for each time region $\vec{x}_t$ we have a d dimensional feature vector $\vec{D}_t = \langle D_{1,t} \cdots D_{d,t} \rangle$ that captures the shape dissimilarity between adjacent time regions.

B. Conditional Neural Fields

Having explained the features that we use, we now provide a preliminary on conditional neural fields [24]. Conditional neural fields is a conditional probabilistic graphical model that combines classical conditional random fields with a single

[1]For instance, the average time taken to run FastDTW and DTW on two 5-sec segments of an X-axis accelerometer reading from the ExtraSensory dataset is 3.76 ms and 20.72 ms respectively, making FastDTW 5.51 times faster than DTW.

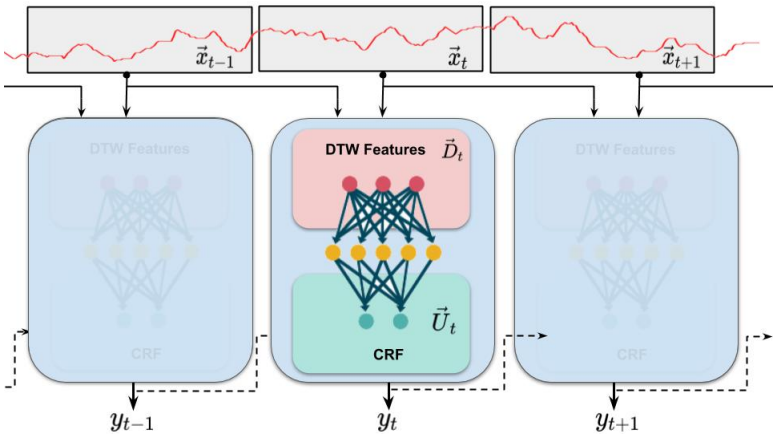

Fig. 1. Overview of the approach

hidden layer neural network. Conditional neural fields was proposed to overcome a limitation of conditional random fields, which fails to model complex non-linear relationships between the input features and the output. The single hidden layer neural network allows such complex relationship to be modelled and captured, leading to a more expressive model. In our context, the neural network takes the shape-based features $\vec{D}_t$ and produces a unary potential vector $\vec{U}_t$:

$$\vec{z}_t = \sigma_1(\vec{\omega}_1^\intercal \vec{D}_t + \vec{b}_1)$$
$$\vec{U}_t = \sigma_{out}(\vec{\omega}_{out}^\intercal \vec{z}_t + \vec{b}_{out})$$

where $\vec{\omega}_1$ and $\vec{\omega}_{out}$ are the weight vectors of the hidden and the output layers respectively; $\vec{b}_1$ and $\vec{b}_{out}$ are the bias vectors of the hidden layer and the output layers respectively; σ_1 and σ_{out} are the activation functions used for the hidden layer and output layers respectively. Figure 1 provides an overview of the approach.

The unary potential vector captures the shape dissimilarity across different dimensions of the time series between two adjacent regions. To capture the temporal relations, conditional neural fields also define a transition potential vector $\vec{T}$, which captures the transition probability between the output states y_{t-1} and y_t. Therefore, we have a set of four parameters to be learnt to obtain these potentials. We let $\vec{w}$ be the combined parameters $\langle \vec{\omega}_1, \vec{\omega}_{out}, \vec{b}_1, \vec{b}_{out}, \vec{T} \rangle$.

Finally, let $\boldsymbol{x} = \langle \vec{x}_t \rangle_{t=1}^m$ and the corresponding hidden state sequence, $\boldsymbol{y} = \langle y_t \rangle_{t=1}^m$, where m is number of time regions in the time series. We define the potential function $\psi_t(\boldsymbol{x}, \boldsymbol{y}; \vec{w})$ capturing the relationship between the input and output states as

$$\psi_t(\boldsymbol{x}, \boldsymbol{y}; \vec{w}) = exp\left(\vec{U}_t \cdot \begin{bmatrix} \mathbb{1}_{y_t=0} \\ \mathbb{1}_{y_t=1} \end{bmatrix} + \vec{T} \cdot \begin{bmatrix} \mathbb{1}_{y_{t-1}=0, y_t=0} \\ \mathbb{1}_{y_{t-1}=0, y_t=1} \\ \mathbb{1}_{y_{t-1}=1, y_t=0} \\ \mathbb{1}_{y_{t-1}=1, y_t=1} \end{bmatrix} \right) \tag{3}$$

.

Then, the conditional distribution of the graphical model is given by

$$P(\boldsymbol{y} \mid \boldsymbol{x}; \vec{w}) = \frac{\prod_{t=1}^m \psi_t(\boldsymbol{x}, \boldsymbol{y}; \vec{w})}{Z(\boldsymbol{x}; \vec{w})}, \tag{4}$$

where $Z(\boldsymbol{x}; \vec{w}) = \sum_{\boldsymbol{y} \in \{\{0,1\}_m\}} \prod_{t=1}^m \psi_t(\boldsymbol{x}, \boldsymbol{y}; \vec{w})$ is the normalization factor.

C. Learning and Inference

The parameters in $\vec{w}$ of the model are learnt and the normalization factor, $Z(\boldsymbol{x}; \vec{w})$, is found by using the forward and backward algorithm, a.k.a belief propagation [38]. Using the α and β table obtained from forward and backward passes we can compute the un-normalized marginal probabilities, $P(y_t = y \mid \vec{x}_t, \vec{x}_{t-1}, y_{t-1}; \vec{w})$ where $y \in \{0, 1\}$ at every time instant t. Let y_{t0} and y_{t1} denote the un-normalised marginal probabilities of y_t being 0 and 1 respectively. Then we use cross entropy loss $\mathcal{L}$ to update the parameter vector $\vec{w}$ using gradient descent. This is given by

$$\mathcal{L}(\vec{w}) = \sum_{t=1}^{m} -y_t \log(y_{t1}) - (1 - y_t) \log(y_{t0}),$$
$$\vec{w'} = \vec{w} - \eta \frac{\partial \mathcal{L}}{\partial \vec{w}},$$

where η is the learning rate and $\vec{w'}$ is the updated weight vector.

After the training process above, we obtained the parameters in $\vec{w}$. Now, as a new test observation segment $\vec{x}_t$ arrives, the optimal $\hat{y}_t$ can be obtained by choosing the $y' \in \{0, 1\}$ that maximizes the conditional distribution

$$\hat{y}_t = \underset{y' \in \{0,1\}}{\operatorname{argmax}} \log P(\hat{y}_t = y' \mid \vec{x}_t, \vec{x}_{t-1}, \hat{y}_{t-1}; \vec{w}).$$

In the equation above, $\vec{x}_t, \vec{x}_{t-1}$ and $\hat{y}_{t-1}$ form the Markov blanket of $\hat{y}_t$. Here, $\hat{y}_t$ is the indicator of whether a change has occurred. To estimate the current state of time series, i.e., change or no change, we require only the previous prediction, the current and the previous observations.

V. Evaluation

In this section, we present the evaluation of Shape-CD on four diverse real-world datasets and analyze its performance under different parameter settings. We also compare Shape-CD against the state-of-the-art time-series change point detection methods.

A. Datasets

We evaluate our approach on four diverse time-series datasets, which are often considered for change point detection. [17], [26].

- **Bee Dance [39]:** This dataset contains the information of the three stage dances honey bees use to communicate the location of pollen and water. Ethologists are interested in identifying the change point from one stage to another. This dataset contains six sequences of the bees position and head-angle.
- **DCASE [40]:** This dataset contains synthetic audio belonging to 11 sound classes in an office settings: clearing throat, coughing, door knock, door slam, drawer, human laughter, keyboard, keys drop, page turning, phone ringing, and speech. It was collected for the DCASE (Detection and Classification of Acoustic Scenes and Events) Challenge of 2016 (Task 2).
- **ExtraSensory [6]:** This dataset consists of 300,000 recorded minutes of sensor data collected from smartphones and smartwatch of 60 participants in the wild. The sensors include accelerometer, gyroscope, magnetometer, audio, location, ambient light, etc. In our evaluation, we use only the tri-axial accelerometer data from the smartwatch. The data has 7 primary labels and 56 secondary labels.
- **Fish Killer [41]:** This dataset contains over 45,000 samples of water level from a dam in Richmond, BC. It helps track the mass loss of fish, which happens when it gets stuck behind the dam. When this phenomenon happens water oscillates in a different manner, which is an indication of a change point.

Further details of these datasets are available in Table I.

TABLE I
Dataset Details

Dataset	Time period (sec)	Domain
Bee Dance	1/15	$\mathbb{R}^3$
DCASE	1/44100	$\mathbb{R}^1$
ExtraSensory	1/25	$\mathbb{R}^3$
Fish Killer	900	$\mathbb{R}^1$

Data cleaning: Since we are only interested in one of the sensors among many in the ExtraSensory dataset, we perform additional data cleaning for this dataset to remove labels along the "flat" inactive regions in the accelerometer data (which likely corresponds to period where the smartwatch is not being worn). Figure 2 shows one such example – the dotted red vertical line is an activity label that is not captured by the smartwatch. In the data cleaning process, we remove the 2nd label onwards along consecutive inactive regions in all three axis. We keep the first label in the inactive regions as it still captures a change point in the activity (such as removing the smartwatch) but due to errors or delay in labelling, the label appears in the inactive regions. The details of the data cleaning process are described in Appendix A.

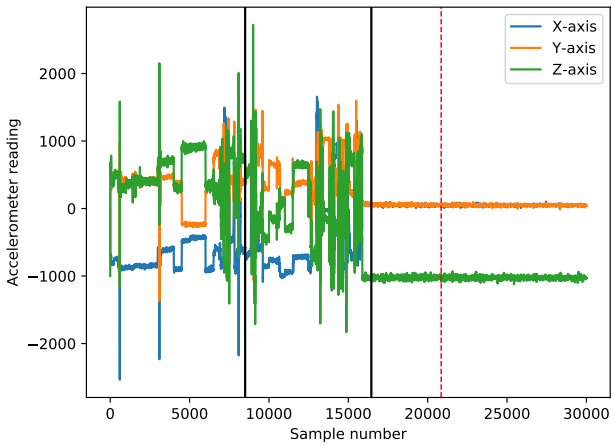

Fig. 2. Example of time-series data of the ExtraSensory data

B. Comparison with Existing Works

We compare Shape-CD with three representative baselines; RuLSIF [17], KL-CPD [26], and LSTM [22], [20]. RuLSIF is a non-parametric unsupervised method, which directly estimates the density ratio and compares the change score obtained using α-relative PE (Pearson divergence) to detect a change. KL-CPD is a recent kernel learning method where the data-specific kernels help in identifying changes. This method has been shown to work in multiple real-world datasets as compared to its deep learning counterparts. LSTM (long short-term memory) is a variant neural network architecture widely used for sequence labelling and classification tasks. Here, we use LSTM as a supervised binary classifier (as done in, e.g., [22]) to label the time segments as "change" or "no change".

We use ROC (Receiver Operating Characteristics) curves and AUC (Area Under the Curve) to measure the performance of the change point detection algorithms [26], [17].

1) Experiment Details: Here we discuss the details regarding the model implementation of Shape-CD and our baseline approaches.

Shape-CD: The input data is segmented into non-overlapping time segments by using a fixed window size and normalised. DTW features are then extracted from these normalised time segments based on Equation 2. We set the window size and relaxation length for the four datasets discussed above using the parameter analysis presented in Section V-D. Next, we label a time segment as a change when

its class label differs from the previous time segments class label. In particular, for ExtraSensory dataset, these activity labels are provided as a combination of secondary and primary labels corresponding to each time segment. Therefore, we consider unique labels by combining the primary and secondary labels. For example, if a time segment is attributed to sitting (primary) and driving (secondary), we combine and refer them as a separate label. Furthermore, in order to combat the data imbalance issue, i.e., the number of positive classes ("change") is much lesser than the negative classes ("no change"), we under sample the data.

Shape-CD is trained using penalised binary cross-entropy loss to help the model balance the prediction between the two classes. We use ReLU (Rectified Linear Units) [42] for σ_1 and Softmax for σ_{out}. We tried different combinations of the activation functions and this combination performs the best. We set the learning rate to 0.01 for all four datasets and we use Adam [43] as the optimiser. The number of hidden layer neurons and optimum train sequence length for each dataset was chosen based on the parameter sensitivity analysis described in Section V-D.

KL-CPD: This method uses an RNN-based Seq2Seq generative model for change detection. To find the parameters that provide optimal performance, we performed hyperparamter tuning for each dataset. The window dimension in a mini-batch was found to be 15 samples for Fish Killer dataset, 10 samples for ExtraSensory dataset, 5 samples for DCASE dataset, and 25 samples for Bee Dance dataset. The coefficient for reconstruction loss was set to 0.001 for all the datasets. The rest of the parameters remained unchanged from the original paper.

LSTM: We use LSTM as a supervised binary sequence classifier to detect changes. The parameters set for implementing this approach was done via hyperparameter tuning. The input to the classifier comprises of time segments with length 5 sec for ExtraSensory dataset, 1 sec for Bee Dance dataset, 10 msec for DCASE dataset, and 8 hrs for Fish Killer dataset. The LSTM model architecture comprises of a single LSTM layer followed by hidden layers using ReLU activation. Sigmoid activation is used at the output. The dimensions of the LSTM and hidden layers set by hyperparameter tuning are shown in Table II. For Fish Killer, we find that the data is simpler (one dimensional, two states), so a dense network does not perform well.

TABLE II
LSTM MODEL ARCHITECTURE DETAILS

Dataset	No. of LSTM units	No. of hidden layers, width
Bee Dance	50	2, 50
DCASE	50	2, 30
ExtraSensory	30	2, 30
Fish Killer	30	0, 0

RuLSIF: We obtain the change scores from the $alpha$ Pearson divergence using the RuLSIF method [17] for all the datasets. The obtained change scores were compared against different thresholds to compute the ROC curves explained in the next section.

We performed 5-fold cross-validation for all the four datasets.

2) ROC analysis: Figure 3 shows the ROC curves of each of the four methods. For supervised methods that use binary classification such as Shape-CD and LSTM in our case, the output probabilities are compared against a threshold of 0.5 by default. To obtain the ROC curve we vary this threshold value chosen by choosing 34 samples, uniformly spaced between 0 and 1. Score obtained from KL-CPD and RuLSIF are also compared against varying thresholds obtained in the same fashion. The AUC values are summarized in Table III.

TABLE III
AUC COMPARISON

Dataset	RuLSIF	LSTM	KL-CPD	Shape-CD
Bee Dance	0.6227	0.6275	0.6029	**0.8937**
DCASE	**0.9997**	0.8606	0.6264	0.9988
ExtraSensory	0.8617	0.6010	0.7737	**0.9305**
Fish Killer	0.6003	0.5402	0.6951	**0.9559**

We can see that Shape-CD shows a notable improvement over the baselines on all the datasets. In the case of the ExtraSensory dataset where the number of output classes are substantial, we can see that KL-CPD fails to perform well as learning the kernel directly from the data generated from complex underlying process is difficult. Similarly, RuLSIF shows degraded performance in this dataset possibly due to the difficulty of capturing a multitude of variations using a pre-defined threshold. LSTM underperforms mainly because it requires a large amount of data to learn and generalise to the varying patterns attributed to a change. Shape-CD, on the other hand, uses representative features to help guide the model learning and displays superior performance with almost 21% higher in AUC for ExtraSensory dataset when compared against KL-CPD.

On average, across all datasets, Shape-CD performs better by 24.7% in AUC than RuLSIF [17], 26.8% better than KL-CPD [26], and 36.7% than LSTM [22].

On the contrary, the DCASE dataset, which consists of just 11 distinguishable labels, becomes a much easier problem to handle. As the distinction between labels is quite pronounced for this data, we can see that RuLSIF is also able to achieve an AUC comparable to Shape-CD. KL-CPD fails to perform here as well due to its inability in handling the multiple classes within the dataset. The benefits of Shape-CD can also be noted in the Bee Dance and Fish Killer datasets where the distinctions in shape of the signal prove to be effective for accurate change detection.

3) Computational Time: In this section, we compare the average time required for each method to predict the output state for a segment. Table IV depicts the average computational time required for RuLSIF, LSTM, KL-CPD and Shape-CD on all four datasets. This average is obtained over 10 runs. For fair comparison, the length of the time segment for each

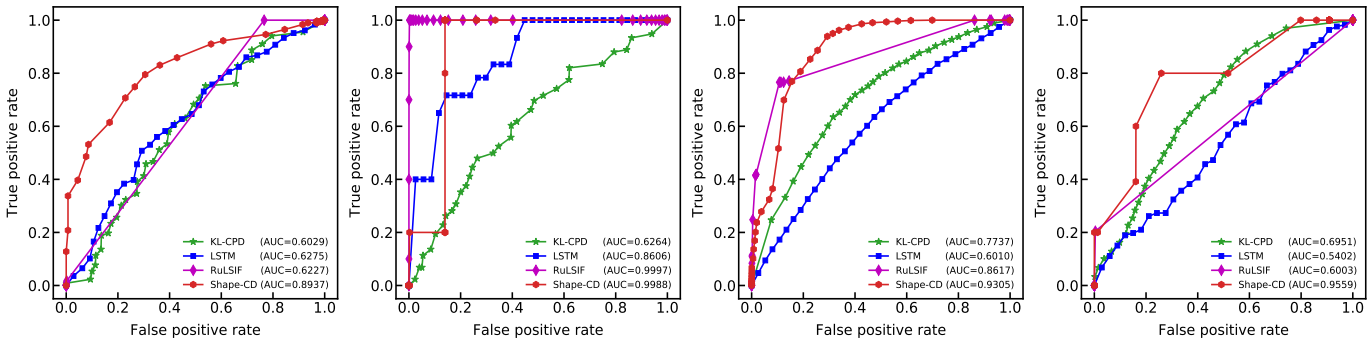

(a) Bee Dance (b) DCASE (c) ExtraSensory (d) Fish Killer

Fig. 3. ROC Curves for Shape-CD (red), RulSIF (green), LSTM(blue) and KL-CPD (magenta).

dataset was set to the optimum window size values obtained in Section V-D. The experiments were conducted on a computer with Intel i7-9750H 2.60 GHz processor with 16 GB RAM running Ubuntu 16.04.

TABLE IV
COMPUTATIONAL TIME PER SEGMENT (MILLISECONDS)

Dataset	RuLSIF	LSTM	KL-CPD	Shape-CD
Bee Dance	10.927	11.382	1.517	**1.397**
DCASE	299.140	81.392	40.964	**17.632**
ExtraSensory	88.835	24.073	12.676	**11.540**
Fish Killer	11.064	8.210	1.725	**0.700**

Our results show that the simplicity of the Shape-CD model results in faster computation compared to the other methods. One of the main factors contributing to Shape-CD's smaller runtime is the calculation of the feature vector using relaxed FastDTW. As the segment length increases, the amount of time taken to compute the DTW features also increases [34]. Apart from this, the runtime is also affected by the width of the hidden layer used for the model. As the width increases, the amount of mathematical operations involved increases in turn causing an increase in the runtime. For instance, in the case of Fish Killer dataset the number of hidden layer neurons is 15 as per experiments conducted in Section V-D, which is the lowest compared to the other datasets. In addition to that, we also note that the length of the time segment for Fish Killer dataset (16 samples) is also lower compared to ExtraSensory dataset and DCASE dataset, making it the fastest among all the datasets.

The runtime for the LSTM model is heavily dependant on the model configuration chosen for each dataset. For instance, the Fish Killer dataset uses the least complex model (with 3781 trainable parameters) as opposed the model used by other datasets such as Bee Dance (15,951 trainable parameters). Increase in input dimension increases the number of mathematical operations between the input layer and the LSTM layer which leads to an increase in the computational time. This is a main reason for the increased prediction time observed in the case of the DCASE dataset (with 12,891 trainable parameters and an input dimension of 441).

RuLSIF is a non-parametric approach, therefore, the runtime variations across datasets can be explained mainly based on the time segment length. Higher segment length leads to more time to compute the change scores which are obtained using α Pearson divergence. KL-CPD computes the Maximum Mean Discrepancy (MMD) scores which uses data-driven kernel function to find changes. In the case of KL-CPD, MMD score is highly dependant on the time segment length. We can see that DCASE runs the slowest as its segment length is the largest amongst all.

C. Training Data Requirement

We now compare the amount of training data required, focusing on the two supervised methods: Shape-CD and LSTM. Shape-CD has a much-less complex model with only 250 trainable parameters for the ExtraSensory dataset, compared to LSTM with 13,291 trainable parameters. Due to this, Shape-CD thus require much less data to train compared to LSTM. Figure 4 depicts the loss convergence graphs of Shape-CD and LSTM models. This graph was taken during the training session of ExtraSensory dataset. We can see that Shape-CD converges after less than 1,500 training samples, while LSTM rqeuires close to 4,000 samples to converge.

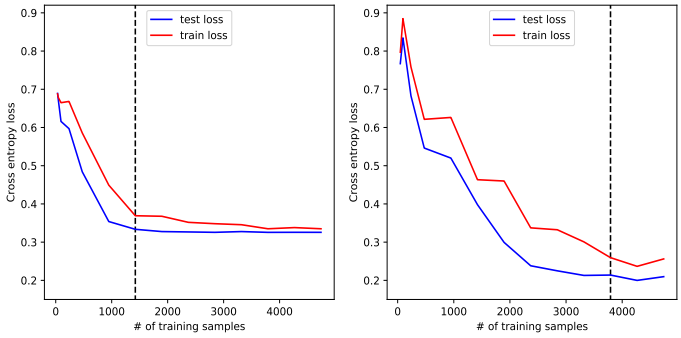

(a) Shape-CD (b) LSTM

Fig. 4. Convergence during Training

D. Parameter Sensitivity Analysis

Finally, we present our experimental results on the effect of various parameters used in Shape-CD to understand the trade-offs.

1) Segment Length: First, we show the performance of our approach by varying the segment length for each dataset. The segment length k affects several factors such as the time granularity, latency of the model prediction, and shape-dissimilarity. Intuitively, shorter segments contain less meaningful patterns since they are more varied within the small duration. On the other hand, longer segment causes an increase in the prediction delay and possibly induce multiple patterns within the same segment, thereby making the shape-dissimilarity measurement more erratic. We compared different segment lengths for all four datasets to observe aforementioned effects on the performance.

Figure 5 shows the ROC curves for Shape-CD under three different segment lengths across all four datasets. Details of the experiment conducted, along with the relaxation parameter r for relaxed FastDTW is illustrated in Table V.

TABLE V
EXPERIMENT PARAMETER

Dataset	Length	r	Optimal segment length
ExtraSensory	1 sec - 10 sec	1 sec	5 sec
Fish Killer	2 hrs - 8 hrs	2 hrs	4 hrs
Bee Dance	0.5 sec - 2 sec	0.5	1 sec
DCASE	5 ms - 20 ms	5 ms	10 ms

We can see that there is a degradation in the performance when we modulate the segment length to its extreme values. A balanced segment length helps yield better performance. The optimum performance was obtained at 5 sec (125 samples) for ExtraSensory dataset, 1 sec (15 samples) for Bee Dance dataset, 10 msec (441 samples) for DCASE dataset, and 4 hrs (16 samples) for Fish Killer dataset.

2) Relaxation Length: We then analyze the effects of the relaxation factor r, which we used in our relaxed FastDTW to obtain the dissimilarity score. Relaxing the end-point constraints in DTW is known to produce better matching between sub-sequences [37]. As our approach is entirely shape-based, achieving the best match is key to the performance of the model. While increasing the relaxation length helps develop flexibility, it also increases the tendency to miss information [36], decreasing the performance. For the relaxation length sensitivity analysis, we use the best segment length obtained from the previous analysis.

Figure 6 shows the ROC curves for Shape-CD under three different r settings across all four datasets. The details for the experiment conducted are depicted in Table VI.

We can see that increasing r results in degraded performance in all the datasets and setting the right amount of flexibility is essential for all the datasets. The optimum performance was obtained at 1 sec (25 samples) for ExtraSensory dataset, 0.5 sec (8 samples) for Bee Dance dataset, 5 msec (220 samples) for DCASE dataset, and 2 hrs (8 samples) for Fish Killer dataset.

TABLE VI
EXPERIMENT PARAMETER

Dataset	r	Segment length	Optimal r
ExtraSensory	0 sec - 2 sec	5 sec	1 sec
Fish Killer	0 hrs - 4 hrs to	4 hrs	2 hrs
Bee Dance	0 sec - 1 sec	1 sec	0.5 sec
DCASE	0 ms - 10 ms	10 ms	5 ms

3) Training Sequence Length: The model trains the time-series data in a sequential manner to learn the temporal connections between the time regions. The length of the train sequence determines the number of neighbouring regions included while training which in turn affects the potentials generated for belief propagation. A higher train sequence length translates to higher model uncertainty due to the increased number of potentials involved in the decision making process. Similarly, if the train sequence length is lower, the model becomes under-informed and shows lower performance.

Figure 7 depicts the model's performance in terms of the AUC measured under varying setting of train sequence length for the four datasets discussed. The optimum performance was recorded when the train sequence length was 5 segments for ExtraSensory dataset, 3 segments for Bee Dance dataset, 5 segments for Fish Killer dataset and 4 segments for DCASE dataset. The black dotted line indicates this information in Figure 7.

4) Number of Hidden Layer Neurons: Shape-CD utilises a single hidden layer neural network that generates the unary potentials required for the graphical model from the measured shape features. The number of neurons chosen to form this layer can impact the model's capability in two ways. First, fewer neurons can result in under-fitting whereas more neurons can result in over-fitting. Second, increasing the number of neurons can make the model unnecessarily complex. This experiment helps us set the width of this layer to its optimum value.

Figure 8 illustrates how the model performs at different widths of the hidden layer for the four datasets discussed. We can see that there is a stark increase in the model performance as the number of neurons increases. After reaching a certain width, however, the performance stagnates. The optimum value corresponds to the width at which this stagnation begins, which is 30 neurons for ExtraSensory dataset, 20 neurons for both Bee Dance and DCASE dataset, and 15 neurons for Fish Killer dataset. The optimum value is indicated as black dotted line in Figure 8.

VI. CONCLUSION

Despite the plethora of work on change point detection in time series data, none of the existing work perform sufficiently well when the data is generated by complex underlying process with large number of unknown states. This shortcoming is often attributed to simplistic assumptions that the current

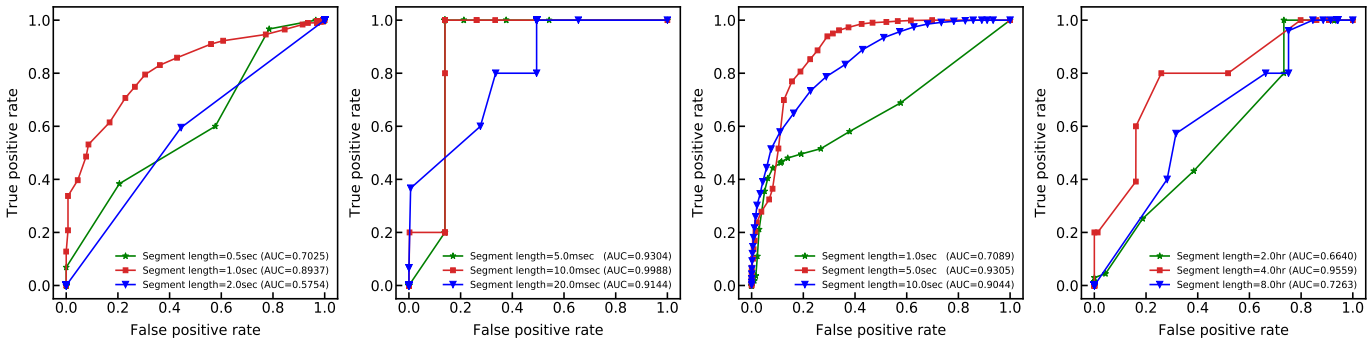

(a) Bee Dance (b) DCASE (c) ExtraSensory (d) Fish Killer

Fig. 5. Effects of Segment Length.

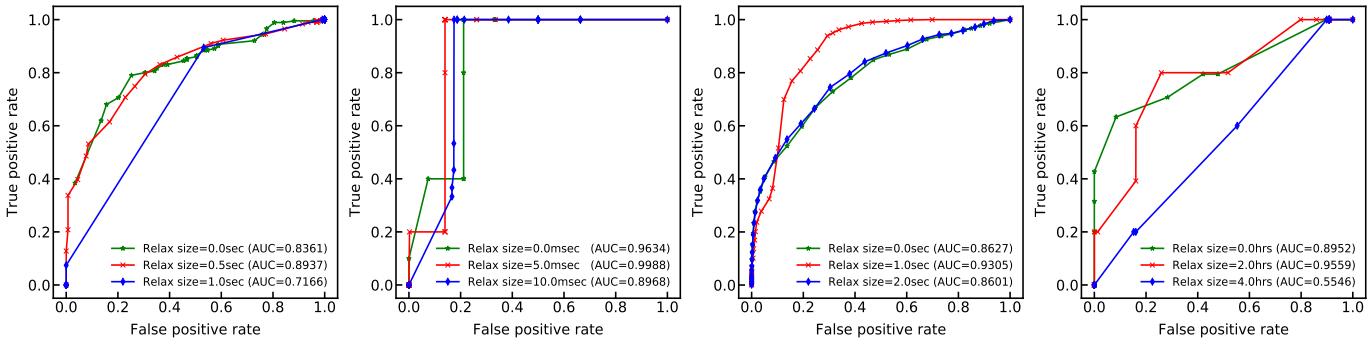

(a) Bee Dance (b) DCASE (c) ExtraSensory (d) Fish Killer

Fig. 6. Effects of relaxation factor.

methods make on the underlying model. Deep learning-based methods, on the other hand, do not make any assumption, but they often result in complex models and require huge amount of training data. We present in this paper, a somewhat surprising solution using what we already know in the literature – we combine shape-based features, which is known to work well, with conditional neural fields, which captures non-linear relationships between the features and the changes. The resulting method, Shape-CD, is both fast, accurate, requires less data to train, and has order of magnitudes fewer parameters to learn than deep learning-based methods. Our work on Shape-CD is motivated by the need to perform change point detection on data generated by complex physical process on IoT devices. The method, however, is general and can be applied to many other scenarios. It performs well even on time series data with a constrained data generation process.

REFERENCES

[1] M. J. Evans and J. W. Malcom, "Automated Change Detection methods for Satellite Data that can Improve Conservation Implementation," *bioRxiv*, p. 611459, 2020.

[2] F. Kaddachi, H. Aloulou, B. Abdulrazak, J. Bellmunt, R. Endelin, M. Mokhtari, and P. Fraisse, "Technological Approach for Behavior Change Detection toward Better Adaptation of Services for Elderly People," in *HEALTHINF*, 01 2017, pp. 96–105.

[3] C. S. Merino, M. Sips, D. A. Keim, C. Panse, and R. Spence, "Task-at-hand Interface for Change Detection in Stock Market Data," in *Proceedings of the working conference on Advanced visual interfaces*, 2006, pp. 420–427.

[4] J.-L. Reyes-Ortiz, L. Oneto, A. Samà, X. Parra, and D. Anguita, "Transition-aware Human Activity Recognition using Smartphones," *Neurocomputing*, vol. 171, pp. 754–767, 2016.

[5] S. Aminikhanghahi and D. J. Cook, "A Survey of methods for Time Series Change Point Detection," *Knowledge and information systems*, vol. 51, no. 2, pp. 339–367, 2017.

[6] Y. Vaizman, K. Ellis, and G. Lanckriet, "Recognizing Detailed Human Context In-The-Wild from Smartphones and Smartwatches," *IEEE Pervasive Computing*, vol. 16, no. 4, pp. 62–74, 2017.

[7] V. Moskvina and A. Zhigljavsky, "An Algorithm Based on Singular Spectrum Analysis for Change-Point Detection," *Communications in Statistics - Simulation and Computation*, vol. 32, no. 2, pp. 319–352, 2003.

[8] Z. Harchaoui, F. Bach, and E. Moulines, "Kernel Change-Point Analysis," in *Proceedings of the 21st International Conference on Neural Information Processing Systems*, ser. NIPS08. Red Hook, NY, USA: Curran Associates Inc., 2008, p. 609616.

[9] G. Nason, *Stationary and Non-Stationary Time Series*, H. Mader and S. Coles, Eds. United Kingdom: Geological Society of London, 2006.

[10] Z. Wu, N. E. Huang, S. R. Long, and C.-K. Peng, "On the Trend, Detrending, and Variability of Nonlinear and Nonstationary Time Series," *Proceedings of the National Academy of Sciences*, vol. 104, no. 38, pp. 14 889–14 894, 2007.

[11] M. Basseville and I. V. Nikiforov, *Detection of Abrupt Changes: Theory and Application*. USA: Prentice-Hall, Inc., 1993.

[12] A. Willsky and H. Jones, "A Generalized Likelihood Ratio approach to the Detection and Estimation of Jumps in Linear Systems," *IEEE Transactions on Automatic Control*, vol. 21, no. 1, pp. 108–112, 1976.

[13] Y. Kawahara, T. Yairi, and K. Machida, "Change-Point Detection in Time-Series Data Based on Subspace Identification," in *Seventh IEEE*

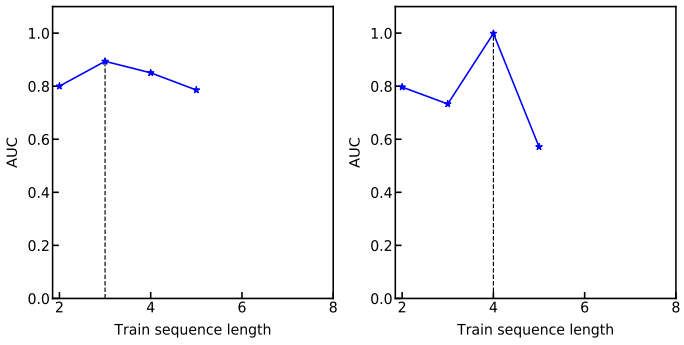

(a) Bee Dance (b) DCASE

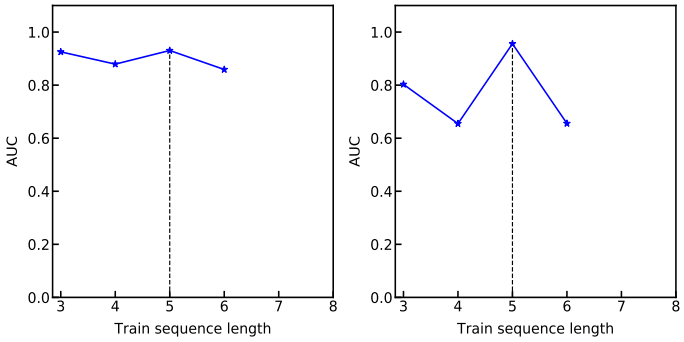

(c) ExtraSensory (d) Fish Killer

Fig. 7. Effect of train sequence length.

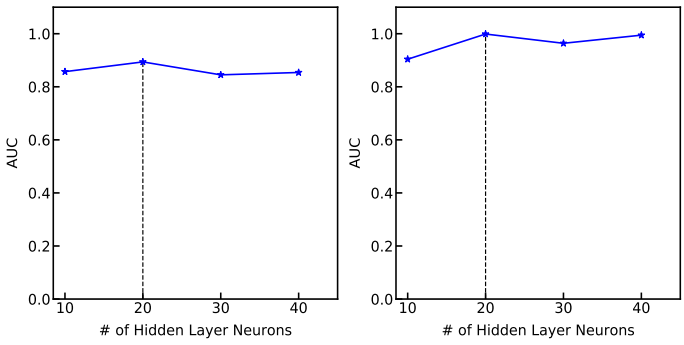

(a) Bee Dance (b) DCASE

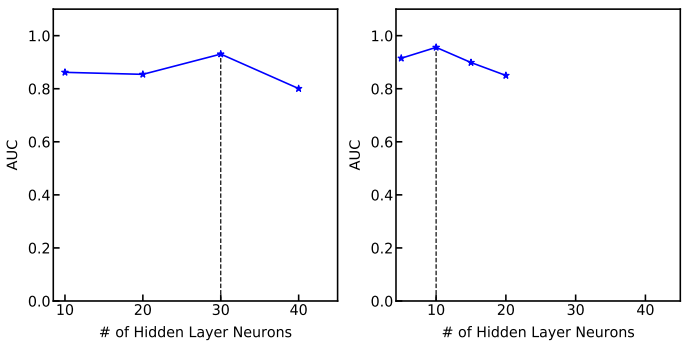

(c) ExtraSensory (d) Fish Killer

Fig. 8. Effect of number of hidden layer neurons.

International Conference on Data Mining (ICDM 2007), Oct 2007, pp. 559–564.

[14] K. Yamanishi and J.-i. Takeuchi, "A Unifying Framework for Detecting Outliers and Change Points from Non-Stationary Time Series Data," in *Proceedings of the Eighth ACM SIGKDD International Conference on Knowledge Discovery and Data Mining*, ser. KDD 02. New York, NY, USA: Association for Computing Machinery, 2002, p. 676681. [Online]. Available: https://doi.org/10.1145/775047.775148

[15] Y. Kawahara and M. Sugiyama, "Sequential Change-Point Detection based on Direct Density-Ratio Estimation," *Statistical Analysis and Data Mining*, vol. 5, no. 2, pp. 114–127, 4 2012.

[16] ——, "Change-Point Detection in Time-Series Data by Direct Density-Ratio Estimation," in *Proceedings of the 2009 SIAM International Conference on Data Mining*. SIAM, 2009, pp. 389–400.

[17] S. Liu, M. Yamada, N. Collier, and M. Sugiyama, "Change-Point Detection in Time-Series Data by Relative Density-Ratio Estimation," *Neural Netw.*, vol. 43, p. 7283, Jul. 2013. [Online]. Available: https://doi.org/10.1016/j.neunet.2013.01.012

[18] I. Cleland, M. Han, C. Nugent, H. Lee, S. McClean, S. Zhang, and S. Lee, "Evaluation of Prompted Annotation of Activity Data Recorded from a Smart Phone," *Sensors*, vol. 14, no. 9, pp. 15 861–15 879, 2014. [Online]. Available: https://www.mdpi.com/1424-8220/14/9/15861

[19] L. Liao, D. Fox, and H. Kautz, "Location-Based Activity Recognition Using Relational Markov Networks," in *Proceedings of the 19th International Joint Conference on Artificial Intelligence*, ser. IJCAI05. San Francisco, CA, USA: Morgan Kaufmann Publishers Inc., 2005, p. 773778.

[20] J. Kim, J. Kim, H. L. T. Thu, and H. Kim, "Long Short Term Memory Recurrent Neural Network Classifier for Intrusion Detection," in *2016 International Conference on Platform Technology and Service (PlatCon)*, 2016, pp. 1–5.

[21] K. D. Feuz, D. J. Cook, C. Rosasco, K. Robertson, and M. Schmitter-Edgecombe, "Automated Detection of Activity Transitions for Prompting," *IEEE Transactions on Human-Machine Systems*, vol. 45, no. 5, pp. 575–585, 2015.

[22] C. Yin, Y. Zhu, J. Fei, and X. He, "A Deep Learning Approach for Intrusion Detection Using Recurrent Neural Networks," *IEEE Access*, vol. 5, pp. 21 954–21 961, 2017.

[23] D. J. Berndt and J. Clifford, "Using Dynamic Time Warping to find Patterns in Time Series." in *KDD workshop*, vol. 10, no. 16. Seattle, WA, 1994, pp. 359–370.

[24] J. Peng, L. Bo, and J. Xu, "Conditional Neural Fields," in *Advances in Neural Information Processing Systems 22*, Y. Bengio, D. Schuurmans, J. D. Lafferty, C. K. I. Williams, and A. Culotta, Eds. Curran Associates, Inc., 2009, pp. 1419–1427. [Online]. Available: http://papers.nips.cc/paper/3869-conditional-neural-fields.pdf

[25] G. Dong and H. Liu, *Feature Engineering for Machine Learning and Data Analytics*, 1st ed. USA: CRC Press, Inc., 2018.

[26] W.-C. Chang, C.-L. Li, Y. Yang, and B. Pczos, "Kernel Change-Point Detection with Auxiliary Deep Generative models," in *International Conference on Learning Representations*, 2019. [Online]. Available: https://openreview.net/forum?id=r1GbfhRqF7

[27] V. N. Vapnik, "An Overview of Statistical Learning Theory," *Trans. Neur. Netw.*, vol. 10, no. 5, p. 988999, Sep. 1999. [Online]. Available: https://doi.org/10.1109/72.788640

[28] J. Paparrizos and L. Gravano, "K-shape: Efficient and Accurate Clustering of Time Series," *SIGMOD Rec.*, vol. 45, no. 1, p. 6976, Jun. 2016. [Online]. Available: https://doi.org/10.1145/2949741.2949758

[29] H. Ding, G. Trajcevski, P. Scheuermann, X. Wang, and E. Keogh, "Querying and Mining of Time Series Data: Experimental Comparison of Representations and Distance Measures," *Proc. VLDB Endow.*, vol. 1, no. 2, p. 15421552, Aug. 2008. [Online]. Available: https://doi.org/10.14778/1454159.1454226

[30] W. Meesrikamolkul, V. Niennattrakul, and C. A. Ratanamahatana, "Shape-Based Clustering for Time Series Data," in *Proceedings of the 16th Pacific-Asia Conference on Advances in Knowledge Discovery and Data Mining - Volume Part I*, ser. PAKDD12. Berlin, Heidelberg: Springer-Verlag, 2012, p. 530541.

[31] J. Paparrizos and L. Gravano, "Fast and Accurate Time-Series Clustering," *ACM Transactions on Database Systems*, vol. 42, no. 2, Jun. 2017. [Online]. Available: https://doi.org/10.1145/3044711

[32] X. Wang, A. Mueen, H. Ding, G. Trajcevski, P. Scheuermann, and E. Keogh, "Experimental Comparison of Representation Methods and Distance Measures for Time Series Data," *Data Min. Knowl.*

Discov., vol. 26, no. 2, p. 275309, Mar. 2013. [Online]. Available: https://doi.org/10.1007/s10618-012-0250-5

[33] X. Xi, E. Keogh, C. Shelton, L. Wei, and C. A. Ratanamahatana, "Fast Time Series Classification Using Numerosity Reduction," in *Proceedings of the 23rd International Conference on Machine Learning*, ser. ICML 06. New York, NY, USA: Association for Computing Machinery, 2006, p. 10331040. [Online]. Available: https://doi.org/10.1145/1143844.1143974

[34] S. Salvador and P. Chan, "Toward Accurate Dynamic Time Warping in Linear Time and Space," *Intell. Data Anal.*, vol. 11, no. 5, p. 561580, Oct. 2007.

[35] R. Wu and E. J. Keogh, "FastDTW is approximate and Generally Slower than the Algorithm it Approximates," 2020.

[36] D. F. Silva, G. Batista, E. Keogh *et al.*, "On the Effect of Endpoints on Dynamic Time Warping," in *SIGKDD Workshop on Mining and Learning from Time Series II*. San Francisco, CA: ACM, 2016.

[37] C. A. Ratanamahatana and E. Keogh, "Three Myths about Dynamic Time Warping Data Mining," in *Proceedings of the 2005 SIAM International Conference on Data Mining*. Newport Beach, CA, USA: SIAM, 2005, pp. 506–510.

[38] L. R. Rabiner, "A tutorial on Hidden Markov models and Selected Applications in Speech Recognition," *Proceedings of the IEEE*, vol. 77, no. 2, pp. 257–286, 1989.

[39] S. M. Oh, J. M. Rehg, T. Balch, and F. Dellaert, "Learning and Inferring Motion Patterns using Parametric Segmental Switching Linear Dynamic Systems," *International Journal of Computer Vision*, vol. 77, no. 1-3, pp. 103–124, 2008.

[40] A. Mesaros, T. Heittola, E. Benetos, P. Foster, M. Lagrange, T. Virtanen, and M. D. Plumbley, "Detection and Classification of Acoustic Scenes and Events: Outcome of the DCASE 2016 challenge," *IEEE/ACM Transactions on Audio, Speech, and Language Processing*, vol. 26, no. 2, pp. 379–393, 2017.

[41] M. Osborne, R. Garnett, K. Swersky, and N. De Freitas, "A Machine Learning approach to Pattern Detection and Prediction for Environmental Monitoring and Water Sustainability," in *Proc. Workshop on Machine Learning for Global Challenges*, 2011.

[42] V. Nair and G. E. Hinton, "Rectified Linear Units Improve Restricted Boltzmann Machines," in *Proceedings of the 27th International Conference on International Conference on Machine Learning*, ser. ICML10. Madison, WI, USA: Omnipress, 2010, p. 807814.

[43] D. P. Kingma and J. Ba, "Adam: A Method for Stochastic Optimization," 2014.

[44] W. H. Press and S. A. Teukolsky, "Savitzky-Golay Smoothing filters," *Computers in Physics*, vol. 4, no. 6, pp. 669–672, 1990.

APPENDIX

A. Data Cleaning: ExtraSensory dataset

We use the tri-axial accelerometer readings from the ExtraSensory dataset. The data cleaning is performed by first smoothing the signal using SavitzkyGolay filter [44]. Denote $\vec{x}, \vec{y}$, and $\vec{z}$ as the smoothed time series signals depicting X-axis, Y-axis and Z-axis of the accelerometer reading respectively. Let Y be the set of ground truth positions provided in the dataset. We like to obtain Y^* which is set of ground truths that needs to be removed. The process of obtaining Y^* is depicted in Algorithm 1.

Algorithm 1: Data Cleaning: ExtraSensory Dataset

Data: $\vec{x}$,$\vec{y}$,$\vec{z}$ and, Y'
Result: Y^* which is the set of position of the ground truths that needs to be removed

$l \longleftarrow 125$;
$Y' \longleftarrow \{\}$;
for $i \in Y$ **do**
  $\vec{x}_b, \vec{x}_f \longleftarrow \{\vec{x_t}\}_{t=i-l}^{i}, \{\vec{x_t}\}_{t=i+1}^{i+l}$;
  $\vec{y}_b, \vec{y}_f \longleftarrow \{\vec{y_t}\}_{t=i-l}^{i}, \{\vec{y_t}\}_{t=i+1}^{i+l}$;
  $\vec{z}_b, \vec{z}_f \longleftarrow \{\vec{z_t}\}_{t=i-l}^{i}, \{\vec{z_t}\}_{t=i+1}^{i+l}$;
end
if $RangeCheck(\vec{x}_b, \vec{x}_f, \vec{y}_b, \vec{y}_f, \vec{z}_b, \vec{z}_f)$ *is true* **then**
  $Y' \longleftarrow Y' + i$;
  else
    if $MeanVarCheck(\vec{x}_b, \vec{x}_f, \vec{y}_b, \vec{y}_f, \vec{z}_b, \vec{z}_f)$ *is true* **then**
      $Y' \longleftarrow Y' + i$;
    end
  end
end
$Y^* \longleftarrow \{\}$;
$K \longleftarrow len(Y')$;
while $j \leq K - 1$ **do**
  $c \longleftarrow = Y'_j$;
  $n \longleftarrow = Y'_{j+1}$;
  $\vec{x}_f, \vec{x}_b, \vec{x}_I \longleftarrow \{\vec{x_t}\}_{t=c-l}^{c+l}, \{\vec{x_t}\}_{t=n-l}^{n+l}, \{\vec{x_t}\}_{t=c-l}^{n+l}$;
  $\vec{y}_f, \vec{y}_b, \vec{y}_I \longleftarrow \{\vec{y_t}\}_{t=c-l}^{c+l}, \{\vec{y_t}\}_{t=n-l}^{n+l}, \{\vec{y_t}\}_{t=c-l}^{n+l}$;
  $\vec{z}_f, \vec{z}_b, \vec{z}_I \longleftarrow \{\vec{z_t}\}_{t=c-l}^{c+l}, \{\vec{z_t}\}_{t=n-l}^{n+l}, \{\vec{z_t}\}_{t=c-l}^{n+l}$;
  if $IntervalCheck(\vec{x}_f, \vec{x}_b, \vec{y}_I, \vec{y}_f, \vec{y}_I, \vec{z}_b, \vec{z}_f, \vec{z}_I)$ *is true* **then**
    $Y^* \longleftarrow Y^* + Y'_{j+1}$;
  end
  $j \longleftarrow j + 1$;
end
return Y^*

The function $RangeCheck$ checks the ranges of the average of the backward and forward slice of the signal. Each axis has a forward and backward slice denoted by p_f and p_b respectively where $p \in \{\vec{x}, \vec{y}, \vec{z}\}$. Each pair of p_f and p_b and is checked whether they fall in a range. It was noted that in ExtraSensory many of the flat regions occur when two of the p_f and p_b, match the condition $\lambda_{b1} \leq \overline{\vec{p}_b} \leq \lambda_{b2}$ and $\lambda_{f1} \leq \overline{\vec{p}_f} \leq \lambda_{f2}$ and the third pair of p_f and p_b matches the condition $\lambda_{b3} \leq \overline{\vec{p}_b} \leq \lambda_{b4}$ and $\lambda_{f3} \leq \overline{\vec{p}_f} \leq \lambda_{f4}$. λ_{b1} and λ_{f1} were set to be -55 and λ_{b2} and λ_{f2} were set to be 55. λ_{b3} and λ_{f3} were set to be -1040 and λ_{b4} and λ_{f4} were set to be -985. The function $MeanVarCheck$ compares the absolute difference of means and absolute difference of standard deviation of the backward and forward slices of all the three axis to a threshold. The difference in means were checked to be within 10 and the difference in standard deviation were set to be within 5 for all the three axis. After applying functions $RangeCheck$ and $MeanVarCheck$ to the three axes we detect the ground truths in the "flat" region from the signal, depicted using Y'.The function $len(Y')$ returns the length of the set Y'.

The function $IntervalCheck$ helps checks for the consecutive ground truth in the flat region, in order to prevent from removing the first ground truth that can be indicative of a change. This is done by comparing the average of the absolute difference between the mean of the slice around consecutive ground truths compared against the interval between them. This was done for all the axes and the threshold of comparison

was to be 4 for all them. All the above mentioned thresholds were obtained by appropriate tuning. The final output which contains the ground truths that needs to be removed which is Y^*